Tunneling conductance in superconductor/ferromagnet junctions: Self-consistent approach

Paul H. Barsic[*,‡] and Oriol T. Valls[†,‡]
School of Physics and Astronomy, University of Minnesota, Minneapolis, Minnesota 55455, USA
(Received 16 June 2008; revised manuscript received 13 November 2008; published 5 January 2009)

We evaluate the tunneling conductance of clean ferromagnet/superconductor junctions via a fully self-consistent numerical solution of the microscopic Bogoliubov-de Gennes equations. We present results for a relevant range of values of the Fermi wave-vector mismatch (FWM), the spin polarization, and the interfacial scattering strength. For nonzero spin polarization, the conductance curves vary nonmonotonically with FWM. The FWM dependence of our results is stronger than that previously found in non-self-consistent calculations since, in the self-consistent case, the effective scattering potential near the interface depends on the FWM. The dependence on interfacial scattering is monotonic. These results confirm that it is impossible to characterize both the FWM and the interfacial scattering by a single effective parameter and that analysis of experimental data via the use of such one-parameter models is unreliable.

DOI: 10.1103/PhysRevB.79.014502 PACS number(s): 74.50.+r, 74.45.+c, 74.78.Fk, 72.25.Mk

I. INTRODUCTION

Refinements in fabrication techniques that have occurred over the past 12 years have made it possible to create devices that exploit and display the interplay between ferromagnetic and superconducting orderings in superconductor/ferromagnet (SF) heterostructures. These developments have raised the possibility of building devices that may be used to manipulate and detect spin-polarized currents. Such devices, besides being of obvious considerable scientific interest, have technological applications for spintronics.[1] It has been suggested that the introduction of an F layer into solid-state qubits may allow a stabilization of the state of the junction without the need for an external field.[2] Study of SF bilayer devices may illuminate the behavior of other systems that undergo spin/charge separation.[3] Spin/charge separation occurs when an electron is injected into a superconductor at the gap edge. The charge is absorbed by the condensate and quickly carried away by the supercurrent while its spin excitation remains.[4] The different spin orderings of the S and F layers lead to spin-dependent transport effects, providing ways to study phenomena such as spin polarization, spin-diffusion lengths, and spin-relaxation times.[5,6] Other potential applications and device geometries are discussed elsewhere.[1,7,8] Earlier work is extensively reviewed in Ref. 9. The knowledge gained from SF spin probes can lead, if the results are properly analyzed, to a better understanding of spin transport properties in different materials and nanostructures.

Thanks to the improved technologies mentioned above, transport in clean SF bilayers is a very active subject of experimental research, but it remains a difficult topic theoretically. The problem of calculating the conductance of an SF bilayer has been solved within the same model we consider here[9,10] but only in a non-self-consistent manner, that is, by assuming the superconducting order parameter to behave as a sharp step function at the interface. This assumption neglects the proximity effect, the "leaking" of superconductivity into the ferromagnet that occurs in real systems. Thus, the proximity effect makes it impossible to identify a precise location where the superconducting correlations end and the ferromagnetic ones begin. Even with this simplification, the non-self-consistent approach is still far from trivial, as one must consider Andreev reflection,[11] the spin asymmetries due to the exchange interaction, and the spin coupling at the interface. Nevertheless, the stark fact remains that neglecting self-consistency of the order parameter amounts to no less than treating SF proximity effects inconsistently. We remedy this situation in this paper, where we show how the difficulties associated with the proximity effect can be overcome and how a self-consistent calculation of the conductance can be achieved. In doing so, we fully account for the influence of the proximity effect, leading to correct, accurate, and more interesting results at the worthwhile cost of having to solve a much more complicated problem. This procedure results in the physical situation of a scattering potential that is dependent on the wave functions of the scattered particles and holes. There is no analytical approach that will give a fully self-consistent pair amplitude for this problem: a numerical approach must be taken. The spatial variations in the pair amplitude complicate the details of Andreev reflection[11] since the density of states (DOS) can no longer be described as having a well-defined BCS gap,[12] and one must consider subgap states and even gapless superconductivity. Since there is no exact analytical solution for the spatial variations in the pair amplitude at an SF interface, there is no analytical solution for the DOS either, nor *a fortiori* for the conductance. In short, this is a complicated four-component scattering problem without an analytical form for the scattering potential. Despite these difficulties, the proximity effect must not be neglected, as it has, as we shall see, a strong influence on the results and on the way experimental data must be analyzed.

Early experimental work[13] was done on devices with an insulating oxide layer between the S and F layers, thus incorporating a superconductor/insulator/ferromagnet (SIF) tunnel junction. The stable oxide layer prevented the diffusion of ferromagnetic impurities into the superconductor, making it possible to work in the clean limit. One disadvantage of SIF systems is that a tunnel barrier inhibits the proximity effect. Another disadvantage of the SIF junction is the reduced spin coherence lengths. While the electrons merely tunnel through the insulator, the strong binding to the lattice

leads to spin decoherence. These tunnel junctions provide good information on the superconducting DOS, but it is dubious whether they provide a good picture of the state of the ferromagnet near the interface, and they will certainly not reveal the consequences of the proximity effect. Other work[14] in a spin transistor geometry demonstrated the possibility of growing SF interfaces over a large area with no insulating oxide layer. The purpose of that study was to explore transverse spin currents, not to examine bilayer conductance at the SF interface. Also, it is not clear that there was no diffusion of magnetic atoms at the interface. More recent[15,16] work has focused on bilayer conductance in planar junctions with sharp interfaces and clean materials. Characteristic peaks in the conductance were observed at bias voltages corresponding to Δ_0, the bulk superconducting gap energy, and an enhanced conductance at zero bias.

Point-contact bilayers offer a convenient method for studying relatively abrupt interfaces.[17–20] These devices are made by growing an oxide layer, thick enough to suppress tunneling, on top of a planar ferromagnet. A small hole is made through the oxide, and a superconductor is grown on top. This geometry prevents diffusion of ferromagnetic atoms during growth and allows for a uniform magnetic field. In this way, it is possible to study experimentally[17,18] the conductance of clean SF bilayers in the ballistic limit. A quicker method for making point contacts mechanically places the tip of a sharpened superconducting wire on a bulk F sample.[6] While such a technique gives poor control over the size and shape of the contact, it is technologically a very desirable procedure as it leads to quickly obtained results, and therefore it may be used to probe the spin states of many different types of F materials. However, the analysis of the data, and of conductance spectroscopy experimental results generally, has been hampered by incomplete understanding of how to relate data and theory. We will extensively address this issue in this work. We will be able to show that there is a clear influence of the proximity effect on transport at SF interfaces, which will enhance our understanding of these devices. This will also show that self-consistent studies are necessary to actually understand these point-contact devices.

In the case of strong interfacial scattering, Andreev reflection and the proximity effect are suppressed. In the limit of a very large interfacial barrier, the conductance reflects essentially the superconducting DOS. If we work with small or medium interfacial barriers, as is the case here, Andreev reflection and the proximity effect become very important, leading to a much more interesting but much more difficult problem. In the small barrier limit Andreev reflection can lead to an enhancement of subgap conductance[9] since a single electron from F must excite a pair of electrons in S. This agrees with experimental observations of zero-bias conductance.[15–18] The proximity effect changes the local DOS (Ref. 21) in the vicinity of the junction, introducing subgap states and even gapless superconductivity.

Semiclassical methods, such as the Eilenberger or Usadel equations,[7,22–24] can give a reasonable approximation to the conductance curves[25] in dirty systems. However, such models are not appropriate for clean systems and can lead to spurious predictions.[15,25] A common phenomenological approach is to define a current polarization parameter[18] based on the difference in spin-up and spin-down DOSs in F. The portion of the transmission coefficient due to the Andreev reflected hole (AR hole) is calculated for an SN interface. Since the AR hole must be in the opposite spin band of the incident electron, the AR hole coefficient is modified by a simple function of the polarization parameter. This is a reasonable phenomenological approach, but it lacks any microscopic justification and is usually of limited success.[19]

There have been many attempts to derive a fully microscopic model to describe the conductance in SF systems.[3,9,10,18,26–32] With the exception of some early work[33] on a tight-binding model, these studies have used an abrupt approximation for the pair amplitude at the interface, thereby focusing on elastic scattering and Andreev reflection but neglecting the proximity effect. These studies do predict some correct qualitative features of the junctions. A self-consistent two-dimensional (2D) tight-binding study[34] has been performed but only to study transport parallel to the interface. The author of Ref. 27 remarks, and we agree, that only a proper consideration of the proximity effect through self-consistent methods will give the correct quantitative features as well.

In this work we show how to numerically calculate conductances of SF bilayers using a fully self-consistent solution to the Bogoliubov-de Gennes (BdG) equations with a net current. We require such a solution to the BdG equations to properly treat clean inhomogeneous systems in three dimensions.[9] We will analyze the resulting eigenfunctions, with proper boundary conditions, and generate transmission probabilities for particles scattered from F to S via the Blonder-Tinkham-Klapwijk (BTK) method.[35] These transmission probabilities can then be used to calculate *I-V* curves, from which we will calculate the conductances. We find good qualitative agreement with experimental results, including an enhanced conductance at zero bias. We show that the Fermi wave-vector mismatch at the interface, the exchange field in the ferromagnet, and the interface barrier scattering all have a significant and independent effect on the shape of the conductance curves. This paper represents the early fruits of a completely different technique, which we expect will eventually be used to study more complicated geometries and conditions. Our solutions will allow for a very careful consideration of the influence of the proximity effect on the conductance, even for very thick F layers.

In Sec. II, we describe in some detail our numerical methods and the procedures that we follow to extract the conductance as a function of applied voltage. The results are presented and discussed in detail in Sec. III. Section IV recapitulates our conclusions and points to future directions.

II. METHODS

The systems we study here are planar junctions made of SF bilayers with atomically smooth interfaces. We assume that the layers are semi-infinite in the directions parallel to the interface (the *x-y* directions). We will take the bands to be parabolic. The superconductor is assumed to be an *s*-wave material. We use a numerical diagonalization of the microscopic Bogoliubov-de Gennes[36] equations for this inhomoge-

neous system. Given a pair potential (order parameter) $\Delta(z)$, to be determined self-consistently, the spin-up quasiparticle $[u_n^{\uparrow}(z)]$ and spin-down quasi-hole $[v_n^{\downarrow}(z)]$ amplitudes obey the BdG equations as follows:

$$\begin{pmatrix} H-h(z) & \Delta(z) \\ \Delta(z) & -[H+h(z)] \end{pmatrix} \begin{pmatrix} u_n^{\uparrow}(z) \\ v_n^{\downarrow}(z) \end{pmatrix} = \epsilon_n \begin{pmatrix} u_n^{\uparrow}(z) \\ v_n^{\downarrow}(z) \end{pmatrix}. \quad (2.1)$$

Here $H=p_z^2/2m-E_F(z)+\epsilon_\perp+U(z)$ is a single-particle Hamiltonian, where $p_z^2/2m$ is the contribution to the kinetic energy from motion in the z direction and $\epsilon_\perp=k_\perp^2/2m$ that corresponds to the x-y variables. The continuous variable $\epsilon_\perp$ is decoupled from the z direction but of course it affects the eigenvalues ϵ_n, which are measured from the chemical potential. We describe the magnetism by an exchange field $h(z)$ which takes the value h_0 in the F material and vanishes in S. As pointed out in Ref. 9, one should not assume that the Fermi wave-vectors k_{FM} and k_{FS} in the F and S materials are the same. We therefore introduce the dimensionless Fermi wave-vector mismatch parameter $\Lambda \equiv (k_{\mathrm{FM}}/k_{\mathrm{FS}})^2 \equiv E_{\mathrm{FM}}/E_{\mathrm{FS}}$. Within the superconducting layer, $E_{\mathrm{F}}(z)$ is equal to E_{FS}, the bandwidth in the S layer (Fermi energy as measured from the bottom of the band), while in the ferromagnet we have $E_{\mathrm{F}}(z)=E_{\mathrm{FM}}$, so that in the F regions the up and down band widths are $E_{\mathrm{F}\uparrow}=E_{\mathrm{FM}}+h_0$ and $E_{\mathrm{F}\downarrow}=E_{\mathrm{FM}}-h_0$, respectively.

We also introduce the dimensionless magnetic strength variable I by $h_0 \equiv E_{\mathrm{FM}} I$. The $I=1$ limit corresponds to the "half-metallic" case. Interfacial scattering is described by the potential $U(z)$ which we take to be of the form $U(z)=H\delta(z-z_0)$, where z_0 is the location of the interface. The dimensionless parameter $H_B \equiv mH/k_{\mathrm{FM}}$ (everywhere in this paper $\hbar=1$) conveniently characterizes the strength of the interfacial scattering. The amplitudes $u_n^{\downarrow}(z)$ and $v_n^{\uparrow}(z)$ can be written down from symmetry relations.[36] We will consider physically relevant values of Λ, I, and H_B. We measure all lengths in terms of the inverse of k_{FS}, the Fermi wave vector in the S material. The dimensionless F width in the z dimension is $D_{\mathrm{F}}=k_{\mathrm{FS}}d_{\mathrm{F}}$, that of S is $D_{\mathrm{S}}=k_{\mathrm{FS}}d_{\mathrm{S}}$, and that of the entire sample is D. The dimensionless spatial coordinates are denoted by $Z=k_{\mathrm{FS}}z$. The pair potential $\Delta(Z)$ must be found through the self-consistent condition,

$$\Delta(Z) = \frac{g(Z)}{2} \sum_n {}' [u_n^{\uparrow}(Z) v_n^{\downarrow}(Z) + u_n^{\downarrow}(Z) v_n^{\uparrow}(Z)] \tanh\left(\frac{\epsilon_n}{2T}\right). \quad (2.2)$$

We will show that we can treat this problem as a plane-wave scattering problem, with a scattering potential that exists over a finite region of space. The scattering potential is, of course, obtained through self-consistent methods. We will then look at the transmitted and reflected waves sufficiently far away from the interaction region so that they, too, are plane waves.[37] In this case, the spatial extent of the scattering potential is governed by the proximity effect. Therefore, we must take the sample size large enough that the pair amplitude is zero over a large fraction of F, and it is approximately equal to its bulk value Δ_0 over a large fraction of S. We call these regions in which the pair amplitude is approximately constant the asymptotic regions. We must also take the total sample size to be very large, so that the minimum wave-vector in the problem, $k_{\mathrm{min}}=\frac{2\pi}{D}$, allows us to approximate a continuum of incident plane waves. In principle, we should take the sample size to be infinite, but we must choose a finite value for computational considerations. We have taken a total sample size of 60 times the superconducting coherence length ξ_0, which turned out to be sufficient to avoid finite-size effects.

The procedure for calculating conductances begins by using the BdG equations (2.1) and the self-consistency condition (2.2) to find a self-consistent order parameter for the system. We use a procedure similar to that in previous work.[8,12,38,39] We start with a fully three-dimensional wave function $\Psi(\mathbf{r})=e^{i\mathbf{k}_\perp\cdot\mathbf{r}}(u(Z),v(Z))^T$. The factor of $e^{i\mathbf{k}_\perp\cdot\mathbf{r}}$ contributes only $\epsilon_\perp=k_\perp^2/2m$, reducing this to a quasi-one-dimensional (1D) problem in the Z direction. We then expand the $u(Z)$ and $v(Z)$ eigenfunctions in a basis of both sines and cosines as follows:

$$\phi_{q\pm}(Z) = \begin{cases} \sqrt{\frac{2}{D}} \cos(k_q Z) \\ \sqrt{\frac{2}{D}} \sin(k_q Z) \end{cases} \quad (2.3)$$

where the $\pm$ signs in the left subindex refer to the sine or the cosine function, respectively. This choice of basis is equivalent to using complex exponentials, but we gain some computational advantage in the very time consuming step of calculating a self-consistent pair amplitude by working with real rather than complex numbers for the time being. The wave vectors k_q are defined in units of k_{FS} as

$$k_q = \frac{2\pi q}{D} \quad (2.4)$$

with q being a positive integer. While the basis in principle requires all $q \geq 0$, in practice it is sufficient to chose a cutoff large enough, so that the largest wave vector in the problem corresponds to an energy that is a few ω_D above the Fermi level. This choice of basis, which implies periodic boundary conditions as needed in this problem, allows for a wave function that is nonzero and has a nonzero first derivative at the boundaries, two necessary conditions for a nonzero current to be present. In this basis, the upper left quadrant of the matrix in the left side of Eq. (2.1) is

$$H_{q+p+}^{+} = \frac{2}{D}(k_q^2+\epsilon_\perp+1)\delta_{pq} + \frac{2}{D}(1-\Lambda-I) \times \left\{ \frac{\sin[(k_p-k_q)D_{\mathrm{F}}]}{k_p-k_q} - \frac{\sin[(k_p+k_q)D_{\mathrm{F}}]}{k_p+k_q} \right\} + \frac{4\sqrt{\Lambda}H_B}{D}[\cos(k_q D_{\mathrm{F}})\cos(k_p D_{\mathrm{F}})+1], \quad (2.5)$$

and the lower right quadrant is

$$H^{-}_{q+p+} = \frac{-2}{D}(k_q^2 + \epsilon_\perp + 1)\delta_{pq} - \frac{2}{D}(1 - \Lambda + I) \times \left\{ \frac{\sin[(k_p - k_q)D_F]}{k_p - k_q} - \frac{\sin[(k_p + k_q)D_F]}{k_p + k_q} \right\} - \frac{4\sqrt{\Lambda}H_B}{D}[\cos(k_q D_F)\cos(k_p D_F) + 1] \quad (2.6)$$

for the cosine terms. For the sine terms,

$$H^{+}_{q-p-} = \frac{2}{D}(k_q^2 + \epsilon_\perp + 1)\delta_{pq} + \frac{2}{D}(1 - \Lambda - I) \times \left\{ \frac{\sin[(k_p - k_q)D_F]}{k_p - k_q} - \frac{\sin[(k_p + k_q)D_F]}{k_p + k_q} \right\} - \frac{4\sqrt{\Lambda}H_B}{D}[\sin(k_q D_F)\sin(k_p D_F)], \quad (2.7)$$

and

$$H^{-}_{q-p-} = \frac{-2}{D}(k_q^2 + \epsilon_\perp + 1)\delta_{pq} - \frac{2}{D}(1 - \Lambda + I) \times \left\{ \frac{\sin[(k_p - k_q)D_F]}{k_p - k_q} - \frac{\sin[(k_p + k_q)D_F]}{k_p + k_q} \right\} + \frac{4\sqrt{\Lambda}H_B}{D}[\sin(k_q D_F)\sin(k_p D_F)]. \quad (2.8)$$

For the cross terms involving a sine and a cosine we have

$$H^{+}_{q+p-} = \frac{2}{D}\left\{ \frac{\cos[(k_p - k_q)D] - \cos[(k_p - k_q)D_F]}{k_p - k_q} - \frac{\cos[(k_p + k_q)D] - \cos[(k_p + k_q)D_F]}{k_p + k_q} \right\} - \frac{2}{D}(\Lambda - I) \times \left\{ \frac{\cos[(k_p - k_q)D_F] - 1}{k_p - k_q} - \frac{\cos[(k_p + k_q)D_F] - 1}{k_p + k_q} \right\} - \frac{4\sqrt{\Lambda}H_B}{D}[\sin(k_q D_F)\cos(k_p D_F)]. \quad (2.9)$$

and

$$H^{-}_{q+p-} = -\frac{2}{D}\left(\frac{\cos[(k_p - k_q)D] - \cos[(k_p - k_q)D_F]}{k_p - k_q} - \frac{\cos[(k_p + k_q)D] - \cos[(k_p + k_q)D_F]}{k_p + k_q} \right) - \frac{2}{D}(\Lambda + I) \times \left\{ \frac{\cos[(k_p - k_q)D_F] - 1}{k_p - k_q} - \frac{\cos[(k_p + k_q)D_F] - 1}{k_p + k_q} \right\} + \frac{4\sqrt{\Lambda}H_B}{D}[\sin(k_q D_F)\cos(k_p D_F)]. \quad (2.10)$$

In the above expressions, the matrix elements are given in units of E_{FS}, i.e., in dimensionless form.

The self-consistency condition [Eq. (2.2)] requires us to calculate the $\langle \phi_p(Z)|\Delta(Z)|\phi_q(Z)\rangle$ matrix elements numerically. The iterative procedure is then to cycle through Eqs. (2.1) and (2.2) until convergence is obtained, as has been explained elsewhere.[8,12,38,39] The very large sizes required for this problem, however, make the computations technically more demanding. It is necessary to massively vectorize all programs in order to obtain results in a reasonable amount of physical time. We have verified that the results for $\Delta(z)$ and other equilibrium quantities coincide with previous ones obtained with real functions and nontransport boundary conditions.

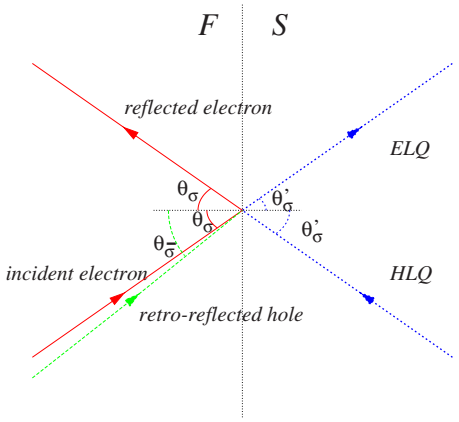

FIG. 1. (Color online) Scattering at an SF interface. An electron is incident from the ferromagnet at an angle θ_σ with spin σ and momentum $\mathbf{k}_\sigma$. Ordinary scattering leads to a partially reflected electron with the same spin and wave vector. For subgap scattering, excitations in the superconductor are Cooper pairs, consisting of an electronlike quasiparticle (ELQ) and a holelike quasiparticle (HLQ) carrying a net spin of zero and charge $2e$. To conserve charge, a hole is retroreflected (Andreev reflection) at an angle $\theta_{\bar{\sigma}}$ into the opposite spin band denoted by $\bar{\sigma}$.

Once we have obtained a fully self-consistent spectrum of eigenfunctions and eigenvalues, we must extract a conductance from them. To successfully apply a plane-wave scattering approach, we require a sample large enough, so that we can assume that the scattering potential is confined to a finite region about the interface and that there are "asymptotic" regions in S and F, far away from the scattering region, where the scattering potential is not felt and the behavior is bulklike. The non-self-consistent work[9] assumes the scattering region to be infinitely small. The general outlines for the self-consistent and non-self-consistent treatments are similar. We will describe here first the salient features of the non-self-consistent treatment and then discuss the changes necessary to study the self-consistent case.

Consider a single electron of spin σ in F with momentum $\mathbf{k}_\sigma$, which is at an angle θ_σ with the Z axis (see Fig. 1). This electron may be partially reflected from the interface as an electron with spin σ and a momentum of the same magnitude, but with the k_z component in the opposite direction (ordinary reflection). Andreev reflection allows a single charge from F to create a Cooper pair excitation in S without violating charge conservation. In this process, when a single electron in spin band σ is incident on the interface, a hole is retroreflected into opposite spin band, which we denote by $\bar{\sigma}$, with momentum $\mathbf{k}_{\bar{\sigma}}$, and a Cooper pair excitation is created in S. We write this as

$$\psi_\sigma(Z) = e^{ik_\sigma Z}\begin{pmatrix}1\\0\end{pmatrix} + a_\sigma e^{ik_{\bar\sigma} Z}\begin{pmatrix}0\\1\end{pmatrix} + b_\sigma e^{-ik_\sigma Z}\begin{pmatrix}1\\0\end{pmatrix}, \tag{2.11}$$

where k_σ and $k_{\bar\sigma}$ indicate the Z components of $\mathbf{k}_\sigma$ and $\mathbf{k}_{\bar\sigma}$, respectively. As noted above Eq. (2.3), $\mathbf{k}_\perp$ is conserved. We normalize to the incident-particle flux and associate the ordinary reflected electron with the b_σ amplitude and the Andreev reflected hole with the a_σ amplitude. The transmitted wave function in S is

$$\psi'_\sigma(z) = c_\sigma e^{ik'_\sigma z}\begin{pmatrix}u_\sigma\\v_{\bar\sigma}\end{pmatrix} + d_\sigma e^{-ik'_\sigma z}\begin{pmatrix}v_{\bar\sigma}\\u_\sigma\end{pmatrix}, \tag{2.12}$$

where c_σ corresponds to an electronlike quasiparticle (ELQ) moving to the right and d_σ corresponds to a holelike quasiparticle (HLQ) moving to the left. The u_σ and $v_{\bar\sigma}$ amplitudes must obey the normalization condition $u_\sigma^2+v_{\bar\sigma}^2=1$. Similar equations can be written down for states with incident holes. We can use the a_σ and b_σ amplitudes to write down a formula for the conductance in the $T\to 0$ limit,[9]

$$G(\varepsilon,\theta) \equiv G_\uparrow(\varepsilon,\theta) + G_\downarrow(\varepsilon,\theta) = \frac{e^2}{h}\sum_\sigma P_\sigma\left(1 + \frac{k_{\bar\sigma}}{k_\sigma}|a_{\bar\sigma}|^2 - |b_\sigma|^2\right), \tag{2.13}$$

where $P_\sigma=(1+\rho_\sigma I)/2$ accounts for the probability for the incident electron to have spin σ,[26] with $\rho_\sigma=1$ for the spin-up band and $\rho_\sigma=-1$ for the spin-down band. The ratio $\frac{k_{\bar\sigma}}{k_\sigma}$ accounts for the different spin band wave vectors. The conductance is a function of the incident angle of the electron from F, $\theta\equiv\theta_\sigma$. While we do not explicitly write it down, a_σ, b_σ, $k_{\bar\sigma}$, and k_σ are functions of ε and θ as well. The angularly averaged conductance is given by[9]

$$G_\sigma(\varepsilon) \equiv \langle G_\sigma\rangle = \frac{\int_0^{\Omega_\sigma} G_\sigma(\varepsilon,\theta)\cos(\theta)d\theta}{\int_0^{\Omega_\sigma}\cos(\theta)d\theta}, \tag{2.14}$$

where Ω_σ is the angle of total reflection (critical angle) for incident particles of spin σ.

This model has the usual features of plane-wave scattering. The conservation of $k_\perp$ across the interface leads to a modified[9] version of Snell's law,

$$k_\sigma \sin(\theta) = k_{\bar\sigma}\sin(\theta_{\bar\sigma}) \tag{2.15}$$

and

$$k_\sigma \sin(\theta) = k'_\sigma \sin(\theta'_\sigma). \tag{2.16}$$

The incident and Andreev reflected angles are, respectively, given by $\sin(\theta)=k_\perp/k_\sigma$ and $\sin(\theta_{\bar\sigma})=k_\perp/k_{\bar\sigma}$. The transmitted angle θ'_σ is found through $\sin(\theta'_\sigma)=k_\perp/k'_\sigma$. This leads to a number of phenomena similar to those in electromagnetic wave scattering. In particular, the critical angle for ordinary reflection, which is given by $\Omega_\sigma=\sin^{-1}(\frac{k'_\sigma}{k_\sigma})=\sin^{-1}(\frac{1}{\sqrt{\Lambda(1+\rho_\sigma I)}})$, depends on the spin band of the incident electron. There is also an angle beyond which Andreev reflection is no longer possible given by $\Omega_{A\sigma}=\sin^{-1}\sqrt{\frac{1+\rho_{\bar\sigma}I}{1+\rho_\sigma I}}$.

The foregoing discussion applies also to the non-self-consistent approach except that Eqs. (2.11) and (2.12) are now possible only in the asymptotic regions far from the interface. The comments that follow are the steps necessary to analyze the self-consistent results. Since there is no condition in the BdG equations to impose a net current traveling to the right, the self-consistent spectrum of eigenfunctions would not be, in the asymptotic regions, in the convenient form of Eqs. (2.11) and (2.12) even if we were to use a basis of complex exponentials. Our choice of periodic boundary conditions allows us to impose the condition of a net current *a posteriori*. This is very similar to the treatment given to one-dimensional scattering problems in elementary quantum mechanics. Since a one-dimensional problem with periodic boundary conditions will produce twofold-degenerate solutions,[40] this quasi-one-dimensional problem also has twofold-degenerate solutions. We can find a linear combination of each pair of degenerate solutions that corresponds to a particle injected into the S layer from the F layer. If we look in the F layer sufficiently far away from the interface (in the asymptotic region), so that the pair amplitude has gone completely to zero, we find that the numerically calculated eigenfunctions can be fit to the form

$$\varphi_\sigma(Z) = \begin{pmatrix}\eta_\sigma \sin(k_\sigma Z + \delta_\sigma)\\ \eta_{\bar\sigma}\sin(k_{\bar\sigma}Z + \delta_{\bar\sigma})\end{pmatrix}. \tag{2.17}$$

Similarly, in the asymptotic region of S, we find

$$\varphi'_\sigma(Z) = \begin{pmatrix}\eta'_\sigma \sin(k'_\sigma Z + \delta'_\sigma)\\ \eta'_{\bar\sigma}\sin(k'_\sigma Z + \delta'_\sigma)\end{pmatrix}. \tag{2.18}$$

If we take a degenerate pair of solutions, $\varphi_{\sigma A}(Z)$ and $\varphi_{\sigma B}(Z)$, they will have the same k_σ and $k_{\bar\sigma}$ but different η_σ, $\eta_{\bar\sigma}$, δ_σ, and $\delta_{\bar\sigma}$, so that they are orthogonal. We can then find a unique linear combination of a pair of degenerate states, $\psi_\sigma(Z)=A\varphi_{\sigma A}(Z)+B\varphi_{\sigma B}(Z)$, that is in the form of Eqs. (2.11) and (2.12) in the asymptotic region. The appropriate complex A and B coefficients are

$$A = \frac{\eta_{\bar\sigma B}e^{i\delta_{\bar\sigma A}}}{\eta_{\sigma A}\eta_{\bar\sigma B}e^{i(\delta_{\sigma A}+\delta_{\bar\sigma A})} - \eta_{\sigma B}\eta_{\bar\sigma A}e^{i(\delta_{\sigma B}+\delta_{\bar\sigma B})}} \tag{2.19}$$

and

$$B = \frac{-A\eta_{\bar\sigma A}}{\eta_{\bar\sigma B}e^{i(\delta_{\bar\sigma B}-\delta_{\bar\sigma A})}}, \tag{2.20}$$

where we have subscripted the parameters to indicate the eigenfunction to which they belong. A small amount of elementary algebra yields expressions for the a_σ and b_σ coefficients, which we can then substitute into Eq. (2.13) to find the conductance.

To find quantities such as k_σ, $k_{\bar\sigma}$, η_σ, $\eta_{\bar\sigma}$, δ_σ, and $\delta_{\bar\sigma}$, we analyze each eigenfunction in the asymptotic region of F. The wave numbers k_σ and $k_{\bar\sigma}$ are quantized in units of $k_{\min}=2\pi/D$ by the discretization of the system. To find their values in each case, we find the zeros of the eigenfunction to

get the characteristic wave number of the eigenfunction and assign it to the nearest multiple of $k_{\min}$. It is then a trivial step to obtain values for δ_σ and $\delta_{\bar{\sigma}}$. Finally, we calculate the amplitudes η_σ and $\eta_{\bar{\sigma}}$ by integrating the square of the eigenfunction over an integer number of periods. We test the quality of our fit by integrating the fit equation with the numerical eigenfunction over an integer number of periods. Each value of a_σ and b_σ depends on both the total-energy value of the state, ε, and the perpendicular wave vector $k_\perp$. To obtain a smooth curve for the conductance, we must have several hundred values of ε. Depending on the critical angles, there will be tens to hundreds of $k_\perp$ corresponding to a single value of ε. The above procedure must therefore be repeated thousands of times to generate a single conductance curve. Since the a_σ and b_σ coefficients, and therefore the conductance, are functions of these numerically obtained quantities, they are subjected to numerical fluctuations arising from the discretization of the k's and numerical errors.

To reduce the influence of numerical fluctuations on the conductance, we use a procedure which has both numerical advantages and which better reflects the physics of the problem. At any temperature, the current is the integral over energies of the conductance,[41]

$$I(V) = \int G(\varepsilon)[f(\varepsilon - eV) - f(\varepsilon)]d\varepsilon \tag{2.21}$$

where $G(\varepsilon)=G_\uparrow(\varepsilon)+G_\downarrow(\varepsilon)$ is the conductance, f is the Fermi function, and V is the bias voltage. At low T, $f(\varepsilon)$ can be approximated by a step function, and it is immediately obvious that the elementary relationship between current and conductance

$$G(V) = \frac{\partial I(V)}{\partial V} \tag{2.22}$$

is not just a definition but a mathematical identity.

It is convenient to numerically evaluate $G(V)$ as follows: after the set of a's and b's have been obtained for all relevant energies and angles, we apply Eqs. (2.13), (2.14), and (2.21) to compute $I(V)$. The integral in the first term of Eq. (2.21) (the second term is independent of V) is evaluated numerically by summing all computed values of $G(\varepsilon)$ from an energy that is a few ω_D below the Fermi energy up to the bias voltage V. The exact value of the lower limit on the integral is not important because it will change the resulting value by a constant which will disappear when Eq. (2.22) is applied. A nonzero lower limit is advantageous because the resulting value will depend on a larger number of states, thus reducing the effects of numerical fluctuations. With this procedure, the value of the integral depends on the conductance for all voltages below V. This has the effect of reducing the influence of numerical fluctuations, resulting in very smooth data, as illustrated by the example given in Fig. 2. The bias voltage is given throughout this work in units of Δ_0/e, so that a dimensionless bias voltage of $V=1$ corresponds to the gap edge, and the normalized current follows from this and the dimensionless definition of G discussed below. This resulting smooth data is then fit to an appropriate simple function. The fit for the $V>1$ and $V<1$ regions are done separately with

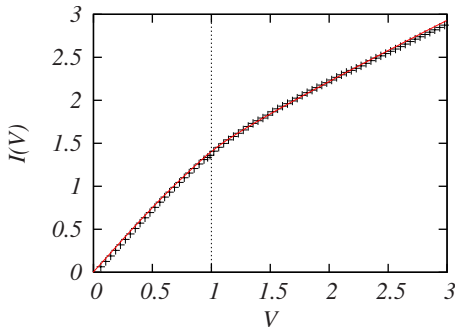

FIG. 2. (Color online) Example of the fitting procedure for the normalized current, as described in the text in connection with Eq. (2.21). The example shown here corresponds to the case $\Lambda=1$ and $I=0.866$, which will be discussed below (Figs. 4 and 5). The crosses are the numerical results obtained as explained in the text and the curves are the fits. The units are explained in the text.

the condition that the first derivative of the current be continuous at $V=1$. The resulting fit is then numerically differentiated to obtain the result for $G(V)$. We follow this procedure for both the forward-scattering and the angularly averaged cases.

III. RESULTS AND ANALYSIS

In this section, we present our numerical results for the conductance of the SF bilayers described above at zero temperature. The materials that form the junction can be characterized by four dimensionless parameters: the exchange field parameter I, the Fermi wave-vector mismatch Λ, the barrier strength H_B, and the dimensionless superconducting coherence length $\Xi_0 \equiv k_{\mathrm{FS}}\xi_0$. We will vary the I and Λ parameters over their physically relevant ranges, which we take to be $0.1 \leq \Lambda \leq 2$ and $0 \leq I \leq 1$ in our units. For the coherence length we choose $\Xi_0=50$ and consider both the case of negligible barrier $H_B=0$ and that of an intermediate barrier $H_B=1$. For stronger interfacial scattering one of course quickly recovers the well-known and less interesting standard tunneling results. Geometrically, we will use values of the dimensionless thicknesses $D_{\mathrm{F}}=D_{\mathrm{S}}=1500$. By calculating conductance curves at a few values of Λ and I for smaller and larger lengths, we have found that the lengths used here are sufficient to avoid finite-size effects. Using a smaller sample size increased numerical fluctuations although it did not change overall trends and averages in the data. We therefore chose the largest sample size that allowed us to calculate high quality numerical results in a reasonable amount of computer time.

Following common convention, dimensionless conductances $G(V)$ are normalized to e^2/h. Thus, for a sample with $\Lambda=1$, $I=0$, $H_B=0$, and $\Delta_0=0$ (a homogeneous nonmagnetic conductor in the normal state), we would obtain $G(V)\equiv 1$. The bias voltage is in units of Δ_0/e; thus, $V=1$ corresponds to the gap edge. We will present results for a range of values of Λ, both smaller and larger than unity, and consider values of the exchange field $I=0.2$, $I=0.5$, and $I=\sqrt{3}/2 \approx 0.866$. Results for $G(V)$ will be given for two cases: forward scattering

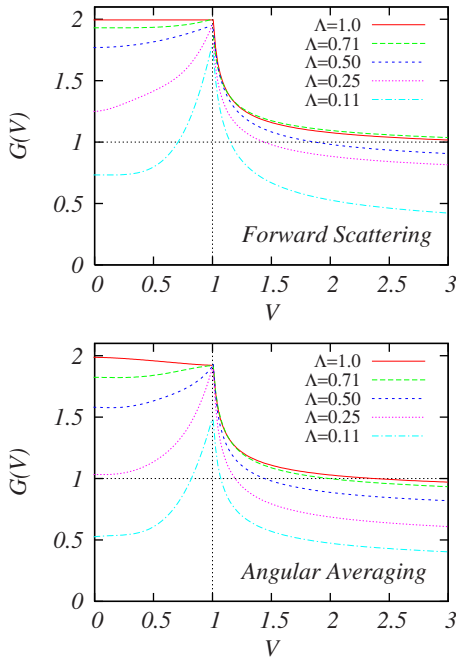

FIG. 3. (Color online) Results for the dimensionless conductance $G(V)$ (see text) as a function of bias voltage V given in units of Δ_0/e. The top panel shows the forward-scattering case for $I=0.2$ and various $\Lambda \leq 1$. The forward conductance is calculated by averaging over an incident-particle flux with angles smaller than $\pi/30$. The bottom panel shows the angularly averaged case at the same values of I and Λ. The conductances are averaged over angles up to the critical angle Ω_σ for spin-up and spin-down particles.

and angularly averaged scattering. For the forward-scattering case, we integrate Eq. (2.14) up to a small angle of $\pi/30$ for spin-up and spin-down incident particles, while the angularly averaged results are integrated up to the maximum possible angle. Forward-scattering results are most applicable to some point-contact devices.

We consider first, in Fig. 3, the behavior of $G(V)$ at a fixed intermediate value of I ($I=0.2$) for several values of Λ in the range of most experimental relevance, $\Lambda \leq 1$. This and subsequent figures are for $H_B=0$, the experimentally more important case of a barrier free junction, which we will study in more detail. Later we will turn to the case where the tunneling limit is approached by setting $H_B=1$. The forward-scattering results are shown in the top panel of Fig. 3. Of the cases shown in this panel, those in the top curve ($\Lambda=1$) serve as a good test of our technique since even with a relatively small exchange field we find results qualitatively similar to the well-established ones obtained by BTK (Ref. 35) at $I=0$. In the BTK approximation, the conductance at zero bias voltage for samples with $I=0$ and $\Lambda=1$ should be equal to 2 due to Andreev reflection, and we see that the top curve in our plot approaches this limit. There, the conductance at $V=0$ is slightly smaller than 2, which is easily explained by a slightly suppressed Andreev reflection due to the different DOSs in the spin-up and spin-down bands at our nonzero I. Furthermore, the conductance asymptotically approaches the normal-state value (unity in these units) at larger bias voltages. We can therefore say that our results approach BTK for $\Lambda=1$ and small I.

The conductance is larger than unity throughout the subgap range for all curves in Fig. 3 except at the smallest Λ. In every case, however, we see that the zero bias conductance is enhanced with respect to the large bias value $G(V \geq 3)$. The value of $G(0)$ monotonically decreases with Λ, which is reasonable because a smaller Λ will lead to stronger ordinary scattering at the interface and inhibited Andreev reflection. If the Andreev reflection and ordinary scattering responded to Λ in the same way, then the ratio of the zero bias conductance to the conductance at larger bias, say $V=3$, would be constant. Instead, we see that the subgap enhancement is considerably reduced for smaller Λ, which implies that Andreev reflection is much more sensitive to Λ than ordinary reflection. The ordering of the conductance curves for $V>1$ is nonmonotonic. The order from greatest to least G is $\Lambda=0.71, 1.0, 0.50, 0.25, 0.11$. This is sensible because the Fermi wave vector for the majority band in the F layer of the $\Lambda=0.71$ curve is equal to 0.85 in units of the Fermi wave vector in S, while that for the $\Lambda=1.0$ curve is 1.2. Therefore, the $\Lambda=0.71$ F layer is slightly better matched to the S than the $\Lambda=1.0$ layer.

The angularly averaged conductance (bottom panel of Fig. 3) is qualitatively similar to that found in the forward-scattering case. The values of the conductances are smaller than in the forward-scattering case because a smaller fraction of the incident current (to which everything is normalized) will pass across the junction. The zero bias enhancement (with respect to the large bias limit) is appreciably less pronounced at smaller Λ. At $\Lambda=0.11$, the value of $G(0)$ is not much larger than $G(3)$. As in the forward-scattering case, the values of $G(1)$ depend strongly on Λ. The $\Lambda=1$ curve in the bottom panel of Fig. 3 shows a very weak conductance peak at a subgap bias. This is a characteristic feature[9] of systems for which the junction characteristics are dominated by the exchange field. For $\Lambda=0.71$, which introduces a small amount of additional ordinary scattering, the conductance peak has completely disappeared. We shall see below that this peak is enhanced with larger I.

The results for a very strong exchange field ($I=0.866$) are shown in Figs. 4 and 5. The first of these figures covers the case where $\Lambda<1$. The strong exchange field makes many features that are already present in Fig. 3 more dramatic. When present, the peaks at subgap biases are proportionally much higher. In the case of $\Lambda=0.25$, there is now a very weak zero bias enhancement in the forward-scattering case and no such enhancement in the angular averaging case. For $\Lambda=0.11$, the suppression of the conductance for subgap bias voltages is very strong. As in the $I=0.2$ case, the ordering of the conductance curves for $V>1$ is nonmonotonic. The order from greatest to least is $\Lambda=0.50, 0.71, 1.0, 0.25, 0.11$. As before, the ordering is dictated by the degree to which the Fermi wave vector of the majority band in F matches the Fermi wave vector in S. In all cases, the value is small because the minority band contributes a minuscule amount to the conductivity.

The next figure (Fig. 5) is for $I=0.866$, as in Fig. 4, but with $\Lambda \geq 1$. Such large values of Λ might be experimentally the case only if the superconducting material were some oxide material with s-wave pairing, but it is nevertheless of theoretical interest. For the two values of $\Lambda>1$ considered

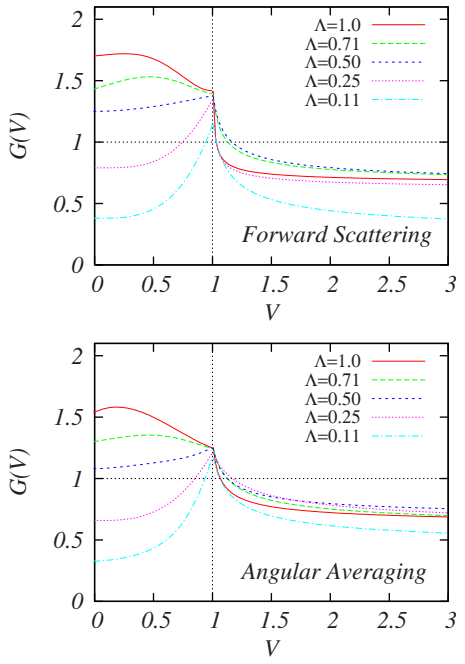

FIG. 4. (Color online) Results for $G(V)$ at a larger value of I than in Fig. 3, $I=\sqrt{3}/2\approx 0.866$, and the same range of Λ. The top panel shows the forward-scattering results and the bottom panel the angularly averaged values. The effects of a strong exchange field are readily apparent when this figure is compared with Fig. 3 (see text).

there we see how the previously observed trends in Λ continue when the mismatch is in the opposite direction. We see that the subgap behavior is monotonic with a marked peak at nonzero bias which is not obtained[9] without self-consistency, and that the conductance is nonmonotonic in Λ for $V>1$.

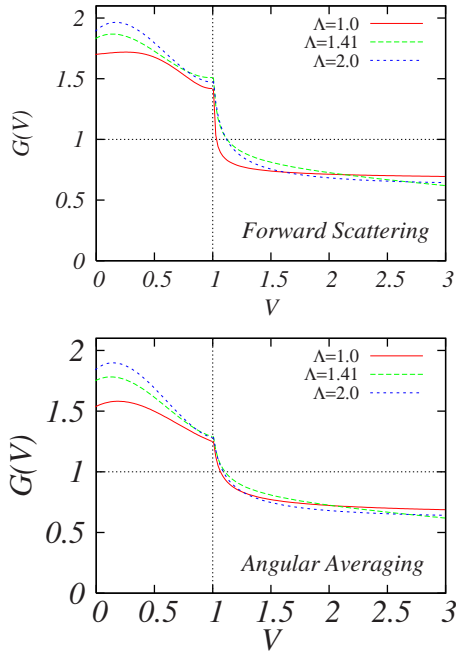

FIG. 5. (Color online) Results for the same case presented in Fig. 4 and with the same panel arrangements but for values of Λ in the range $\Lambda\geq 1$. See text for discussion.

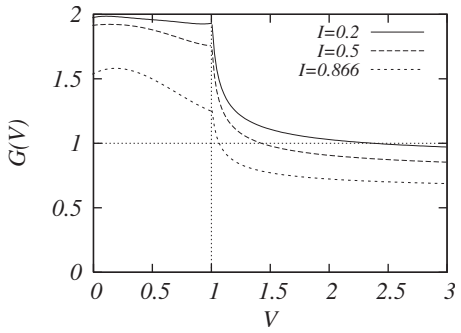

FIG. 6. Angularly averaged values of $G(V)$ for various I at the same $\Lambda=1.0$. This figure shows (see text) that stronger I suppresses both ordinary scattering and Andreev reflection. Note that $G(0)/G(3)\approx 2$ for all values of I shown here and that $G(0)/G(1)$ increases with increasing I.

In Fig. 6, we consider the effect of changing I at constant Λ. The mismatch is held to $\Lambda=1$ and the exchange field is taken from a moderate $I=0.2$ to a strong $I=0.866$. We chose to show the angularly averaged case because the subgap conductance peak is more apparent than in the forward-scattering case. The $I=0.2$ curve, which was discussed above, appears nearly flat when in the company of curves with larger I. For $I=0.5$, the conductance peak is a little more pronounced. Overall, the conductance is smaller as I increases because a larger exchange field leads to more poorly matched Fermi wave vectors from F to S. The $I=0.866$ conductance curve is the most dramatic. The value at zero bias is proportionally much larger than $G(1)$ than for $I=0.5$ or $I=0.2$. The ratio of the zero bias conductance to the conductance at larger bias voltages is approximately two for all values of I shown here. This contradicts the common assertion that the reduction in the minority-band DOS invariably leads to a smaller Andreev reflection.

In all figures shown thus far, the cusp in the conductance for bias voltages corresponding to the gap edge is dependent on both Λ and I. The non-self-consistent analysis[9] leads to an analytical prediction that the value of $G(1)$ depends on I but not on Λ, namely,

$$G(V=1;I)=\frac{4(1-I^2)^{1/2}}{1+(1-I^2)^{1/2}}. \tag{3.1}$$

This result depends very strongly on the assumption that the order parameter is independent of Λ, an assumption which is not valid particularly near the interface,[39] when the order parameter is calculated self-consistently. By comparing the results reported here to Eq. (3.1), one can easily gauge the importance of the effects of self-consistency. Figure 7 is a direct comparison between the non-self-consistent formula[9] for $G(V=1;I)$ [Eq. (3.1)] and the self-consistent results. The figure shows $G(V=1;I)$ for $I=0.2$ (top panel) and $I=0.866$ (bottom panel). The results for $I=0.2$ are plotted in the range of Λ included in Fig. 3 and those for $I=0.866$ in the more extended range included in Figs. 4 and 5. The non-self-consistent results, which are, as explained above, independent of Λ, are shown as the horizontal lines. The self-consistent results are the data points. The error bars represent

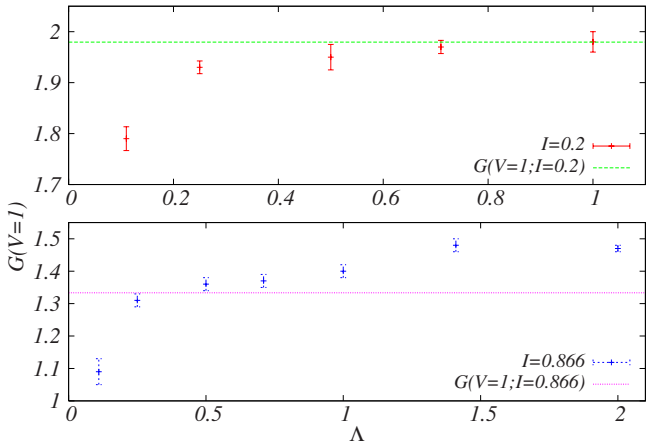

FIG. 7. (Color online) Plots of $G(I;V=1)$, the value of the dimensionless conductance at $V=1$, in the forward-scattering case for $I=0.2$ (top panel) and $I=0.866$ (bottom panel). The horizontal lines labeled by $G(V,I)$ show the result from the non-self-consistent formula [Eq. (3.1)]. The points represent the numerical results from the present self-consistent study at the values of I indicated in the legend. The error bars represent the uncertainty in the numerically obtained values (see text). Note the different horizontal range included in the upper and lower panels. This figure shows that there is an increase in $G(V=1)$ with increasing Λ, a trend which is not obtained without a fully self-consistent pair amplitude.

the numerical uncertainty which arises because $G(V)$ has a sharp cusp at $V=1$. This discontinuous first derivative at $V=1$ makes this the most difficult value of the conductance to obtain numerically, but it is experimentally useful. Even with the numerical error, the difference between the two methods is apparent. There is a clear increasing trend in the self-consistent results as a function of Λ, a sharp contrast with the Λ-independent value predicted by the non-self-consistent result. This trend is stronger at larger I. This large discrepancy is due, as mentioned above, to the fact that the non-self-consistent result relies on the assumption that Δ is independent of Λ. Discrepancies of similar order are also seen at other values of V. These quantitative differences are in addition to qualitative ones such as those discussed in connection with Fig. 5. It should not come as a surprise that the self-consistent results for G are so different from the non-self-consistent ones since, near the interface, $\Delta(z)$ is very different from the non-self-consistent (that is the bulk) value. It seems, though, that the effect of this difference on the result for $G(V=1)$ is minimized when the mismatch is at a minimum. This is, however, rarely the experimental situation: for most materials of experimental interest there is considerable mismatch.

In the non-self-consistent treatment, it was found that the Fermi wave-vector mismatch Λ has an important effect on the conductance curves.[9] In this section, we have shown that the effect of Λ is even greater when self-consistency is included. It is a common experimental practice[42,43] to characterize conductance curves by using some set of parameters (e.g., I, H_B, and Δ_0) which does not include Λ. One uses such fits to experimental results for $G(V)$ to extract I, the unknown polarization of the F electrode. The size of the variation in $G(V)$ with Λ, up to 35% from the smallest to the

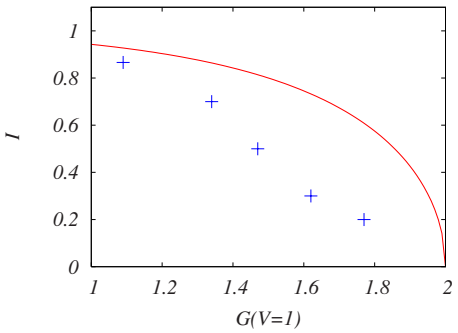

FIG. 8. (Color online) Illustration of the large difference between the value of the I parameter that would be obtained from analyzing experimental data using the non-self-consistent results (Ref. 9) and those obtained from the correct self-consistent analysis. The inferred value of I is plotted vs the measured value of $G(1)$. The non-self-consistent (analytical) results are the solid curve and the self-consistent ones the data points. See text for details.

largest values at $V=1$ as shown in Fig. 7, is such that even (see, e.g., Fig. 6) a 10% variation in $G(V=1)$ corresponds to a large change in I. In light of the results in Ref. 9, confirmed and reinforced here, neglecting Λ is a deplorable practice and can easily lead to spurious results. A much sounder procedure would be to fit results for different samples using Λ, H_B, and I as fitting parameters, taking Δ_0 as the value of the bulk material and disentangling the effects of Λ and H_B by remembering that the latter, but not the former, will change from junction to junction.

The difference between self-consistent and non-self-consistent results that we have found here has additional profound implications for the experimental study of SF junctions. As just mentioned, $G(V)$ data from such junctions are used experimentally to quickly characterize material parameters of the junction, most notably the strength I of the magnet, which is otherwise very difficult to access experimentally. To do this the $G(V)$ data must be fit to the appropriate model. A serious difficulty in doing this is that the curves are simple and the parameters available are many. In addition to microscopic parameters, such as I, Δ_0, or Λ, experimentalists also have overall normalizations and even phenomenological "broadening" parameters (see, e.g., Γ of Ref. 44) at their disposal. Therefore it turns out to be quite possible, even easy, to fit the same data to different models but with ensuing widely different values of I. This is starkly shown, among other places, in Fig. 6 of Ref. 20 where the same data are fit to three different phenomenological models, resulting in three inferred values of I, differing from each other by up to 50%. Therefore, even the most careful analysis of experimental data will produce nonsense if an incorrect model is used.

It is therefore fundamental to choose the correct model if one is to have any hope of obtaining the correct material parameters. In Fig. 8, we illustrate that very serious errors in the determination of I will ensue from using the non-self-consistent theory, rather than the correct self-consistent one, to fit experimental data. We assume for these purposes a value of $\Lambda=0.11$, which is appropriate for a narrow-band magnet in contact with a good metallic superconductor. If the

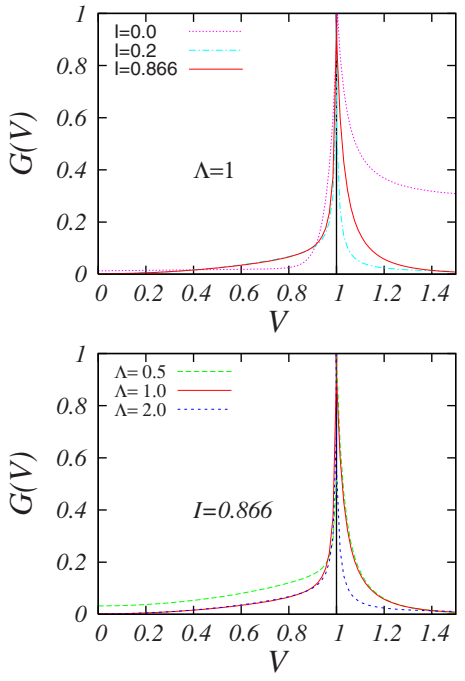

FIG. 9. (Color online) The conductance at interface scattering value $H_B=1$ near the tunneling regime. All results correspond to the forward-scattering case. The top panel shows $G(V)$ for three values of I at $\Lambda=1$, while the bottom panel shows $G(V)$ at $I=0.866$ for three values of Λ.

barrier is clean, which can be determined from the values of $G(V)$ at small V (see below), then the parameters to be determined from the fit would be Δ_0, which would follow from the position of the finite bias cusp, and I, which would have to be inferred from the values of G near $V=1$. In Fig. 8 we plot (solid line) the non-self-consistent result [from inverting Eq. (3.1)] giving the inferred value of I in terms of the experimentally measured value $G(V=1)$. The data points are our self-consistent numerical results. We see then that the results are very different. For example, an experimental value of $G(1)=1.78$, which correctly corresponds to a weak magnetic polarization $I=0.2$, would be misinterpreted as implying $I=0.60$, a much stronger magnet and an error by a factor of 3. One should physically expect such discrepancies since the self-consistent pair potential near the boundary is quite different from the step function of the non-self-consistent theory.[39] Hence, the use of a non-self-consistent theory can easily lead to disastrous errors, and using the self-consistent theory is mandatory if material parameters are to be reliably deduced.

All of the previous results shown have been obtained in the regime of most experimental interest where the interfacial scattering parameter H_B is negligible. In the next figure (Fig. 9) we present results for $H_B=1$, when the tunneling regime ($H_B \gg 1$) is approached, as can be seen from the very different shape of the curves. The two panels in the figure display both the dependence of the results on I at constant Λ (top panel) and the dependence on Λ at constant I (bottom panel). In general, these dependences are not strong. This is because in the true tunneling regime $G(V)$ simply reflects the superconducting DOS and, as one approaches this regime, this should of course result in a weaker Λ dependence. This is well known to experimentalists: to obtain reliable measurements of quantities such as the polarization parameter, it is always preferable to work with samples that have small interfacial scattering. In other words, a larger H_B inhibits Andreev reflection and the proximity effects.

Nevertheless, at $H_B=1$ some definite trends can be ascertained and definite statements can be made. In the top panel of Fig. 9 one can see that the I dependence at constant Λ is still relatively strong, particularly in the region $V>1$. It is remarkable that the behavior with I is strongly nonmonotonic at larger voltages and also, although much more weakly, at $V<1$. This makes interpolation schemes very doubtful in interpreting experimental data. In the bottom panel, corresponding to a strong magnet, we see that the mismatch dependence is weak in the region $V>1$ for $\Lambda \leq 1$ but quite noticeable for $\Lambda>1$. In the region $V<1$ the situation is exactly the opposite: the curves corresponding to $\Lambda=1$ and $\Lambda=2$ nearly coincide, while that for smaller Λ is clearly different. This nonmonotonic behavior contrasts again with that found in non-self-consistent results [see, for example, panel (b) of Fig. 2 in Ref. 9] which, for similar values of I, vary monotonically[45] with mismatch in the same way over the whole range of V.

IV. CONCLUSIONS

We have introduced a method for calculating conductances in an FS bilayer within a fully self-consistent microscopic model. Many of the features that we find are seen in experimental work. There is a subgap enhancement of the conductance, the conductance does approach the normal-state value for larger bias voltages, and there is a cusp at bias voltages of unity. Most important, we show that, as already indicated by the non-self-consistent results, detailed experimental analysis (in particular the extraction of the spin polarization) is impossible if one does not take into account separately the effects of mismatch and those of barrier scattering.

The features of the conductance curves are superficially similar those obtained via non-self-consistent procedures; there are however qualitative and strong quantitative differences. This is clearly illustrated by our study of the dependence of $G(V)$ on Λ and I. Most telling is the strong dependence of $G(V)$ on the Fermi wave-vector mismatch parameter Λ. In the non-self-consistent approach, $G(V \equiv \Delta_0)$ is analytically found[9] to be independent of Λ, while here we find that this quantity shows a monotonically increasing trend, varying by more than 35% over the range of Λ we study. Unlike the non-self-consistent results, we find that the subgap conductance is reduced for smaller Λ and larger I. We find a subgap conductance peak for strong I and Λ close to unity. All of this indicates that, while the non-self-consistent approach is a good tool to help us understand qualitatively some of the features of SF transport, a fully self-consistent approach is needed to properly model experimental data.

The importance of including self-consistency in analyzing experimental results must be re-emphasized. We have seen

how, as reported in the literature, it is easy to extract[20] very different values of the parameter I from good fits of the same data to at least three different models. The problem is that such a physically significant parameter is experimentally inaccessible, and its value must be inferred from such fits. The key issue in this paper is not to introduce an additional set of parameters to which the data can also be fitted; to think this would be to misunderstand its purpose. Our point is that the correct self-consistent treatment of the proximity effect makes a very important quantitative difference in the value of the fitting parameters; that is, in the extracted values of the material properties one is trying to infer from the measurements. We have explored the influence of the proximity effect, which is not directly observable, on the conductance of bilayer junctions. We have developed a method wherein the conductance is calculated while correctly taking the proximity effect into account and compared it to a model which is equivalent in all respects but neglects self-consistency. Based on this comparison, it is clear that the proximity effect should be taken into account self-consistently when analyzing experimental data. Failure to do so makes experimental results simply unreliable. It must also be included in developing future models.

This paper represents merely the first step in studying SF bilayers using a fully self-consistent pair amplitude. Future work may involve the addition of normal-metal electrodes at the boundaries of the sample, allowing us to explore the effects of finite F and S widths. Detailed studies of the relationship between the local densities of states (DOSs) and the conductance are also desirable. Finally, the effects of finite temperature should be explored.

ACKNOWLEDGMENTS

We are very grateful to Klaus Halterman for many discussions on the technical aspects of this numerical work and to Igor Žutić for numerous conversations on this problem.

*Present address: Areté Associates, 1550 Crystal Dr. Ste. 703, Arlington, Virginia 22202, USA; pbarsic@arete.com
†otvalls@umn.edu
‡Also at Minnesota Supercomputer Institute, University of Minnesota, Minneapolis, Minnesota 55455, USA.

[1] I. Žutić, J. Fabian, and S. Das Sarma, Rev. Mod. Phys. **76**, 323 (2004).
[2] G. Blatter, V. B. Geshkenbein, and L. B. Ioffe, Phys. Rev. B **63**, 174511 (2001).
[3] S. Kashiwaya, Y. Tanaka, N. Yoshida, and M. R. Beasley, Phys. Rev. B **60**, 3572 (1999).
[4] B. Leridon, J. Lesueur, and M. Aprili, Phys. Rev. B **72**, 180505(R) (2005).
[5] T. Yamashita, S. Takahashi, H. Imamura, and S. Maekawa, Phys. Rev. B **65**, 172509 (2002).
[6] R. J. Soulen, Jr., J. M. Byers, M. S. Osofsky, B. Nadgorny, T. Ambrose, S. F. Cheng, P. R. Broussard, C. T. Tanaka, J. Nowak, J. S. Moodera, A. Barry, and J. M. D. Coey, Science **282**, 85 (1998).
[7] A. I. Buzdin, Rev. Mod. Phys. **77**, 935 (2005).
[8] K. Halterman and O. T. Valls, Phys. Rev. B **72**, 060514(R) (2005).
[9] I. Žutić and O. T. Valls, Phys. Rev. B **61**, 1555 (2000).
[10] I. Žutić and O. T. Valls, Phys. Rev. B **60**, 6320 (1999).
[11] A. F. Andreev, Sov. Phys. JETP **19**, 1228 (1964).
[12] K. Halterman and O. T. Valls, Phys. Rev. B **69**, 014517 (2004).
[13] R. Meservey and P. Tedrow, Phys. Rep. **238**, 173 (1994).
[14] M. Johnson, Appl. Phys. Lett. **65**, 1460 (1994).
[15] S. Reymond, P. SanGiorgio, M. R. Beasley, J. Kim, T. Kim, and K. Char, Phys. Rev. B **73**, 054505 (2006).
[16] S. Hacohen-Gourgy, B. Almog, and G. Deutscher, Appl. Phys. Lett. **92**, 152502 (2008).
[17] P. Raychaudhuri, A. P. Mackenzie, J. W. Reiner, and M. R. Beasley, Phys. Rev. B **67**, 020411(R) (2003).
[18] S. K. Upadhyay, A. Palanisami, R. N. Louie, and R. A. Buhrman, Phys. Rev. Lett. **81**, 3247 (1998).
[19] F. Pérez-Willard, J. C. Cuevas, C. Sürgers, P. Pfundstein, J. Kopu, M. Eschrig, and H. v. Löhneysen, Phys. Rev. B **69**, 140502(R) (2004).
[20] P. Chalsani, S. K. Upadhyay, O. Ozatay, and R. A. Buhrman, Phys. Rev. B **75**, 094417 (2007).
[21] K. Halterman and O. T. Valls, Physica C **397**, 151 (2003).
[22] M. Krawiec, B. L. Györffy, and J. F. Annett, Phys. Rev. B **66**, 172505 (2002).
[23] M. Leadbeater, C. J. Lambert, K. E. Nagaev, R. Raimondi, and A. F. Volkov, Phys. Rev. B **59**, 12264 (1999).
[24] R. Seviour, C. J. Lambert, and A. F. Volkov, Phys. Rev. B **59**, 6031 (1999).
[25] G. P. Pepe, R. Latempa, L. Parlato, A. Ruotolo, G. Ausanio, G. Peluso, A. Barone, A. A. Golubov, Ya. V. Fominov, and M. Yu. Kupriyanov, Phys. Rev. B **73**, 054506 (2006).
[26] M. J. M de Jong and C. W. J. Beenakker, Phys. Rev. Lett. **74**, 1657 (1995).
[27] N. Stefanakis, Phys. Rev. B **64**, 224502 (2001).
[28] R. Mélin, Europhys. Lett. **51**, 202 (2000).
[29] G. Tkachov, E. McCann, and V. I. Fal'ko, Phys. Rev. B **65**, 024519 (2001).
[30] J. Cayssol and G. Montambaux, Phys. Rev. B **71**, 012507 (2005).
[31] M. Božović and Z. Radović, Phys. Rev. B **66**, 134524 (2002).
[32] J. Linder and A. Sudbø, Phys. Rev. B **75**, 134509 (2007).
[33] J. X. Zhu and C. S. Ting, Phys. Rev. B **61**, 1456 (2000).
[34] K. Kuboki and H. Takahashi, Phys. Rev. B **70**, 214524 (2004).
[35] G. E. Blonder, M. Tinkham, and T. M. Klapwijk, Phys. Rev. B **25**, 4515 (1982).
[36] P. G. de Gennes, *Superconductivity of Metals and Alloys* (Addison-Wesley, Reading, MA, 1989).
[37] E. Merzbacher, *Quantum Mechanics*, 2nd ed. (John Wiley & Sons, New York, 1970).
[38] P. H. Barsic, O. T. Valls, and K. Halterman, Phys. Rev. B **75**, 104502 (2007).
[39] K. Halterman and O. T. Valls, Phys. Rev. B **65**, 014509 (2001).

[40] J. W. Brown and R. V. Churchill, *Fourier Series and Boundary Value Problems*, 6th ed. (McGraw-Hill, New York, 2001).
[41] S. Datta, *Electronic Transport in Mesoscopic Systems* (Cambridge University Press, Great Britain, 1995).
[42] L. Wang, T. Y. Chen, and C. Leighton, Phys. Rev. B **69**, 094412 (2004).
[43] L. Wang, T. Y. Chen, C. L. Chien, J. G. Checkelsky, J. C. Eckert, E. D. Dahlberg, K. Umemoto, R. M. Wentzcovitch, and C. Leighton, Phys. Rev. B **73**, 144402 (2006).
[44] E. M. González, A. D. Folgueras, R. Escudero, J. Ferrer, F. Guinea, and J. L. Vicent, New J. Phys. **9**, 34 (2007).
[45] The mismatch parameter L_0 used in Ref. 9 is related to Λ as $L_0^2 = 1/\Lambda$.